Microwave-assisted reactive sintering and lithium ion conductivity of Li 1.3 Al 0.3 Ti 1.7 (PO 4) 3 solid electrolyte

Leopold Hallopeau, Damien Bregiroux, Gwenaëlle Rousse, David Portehault, Philippe Stevens, Gwenaëlle Toussaint, Christel Laberty-Robert

Microwave-assisted reactive sintering and lithium ion conductivity of $Li_{1.3}Al_{0.3}Ti_{1.7}(PO_4)_3$ solid electrolyte

Leopold Hallopeau[a], Damien Bregiroux[a,*], Gwenaëlle Rousse[b], David Portehault[a], Philippe Stevens[c], Gwenaëlle Toussaint[c], Christel Laberty-Robert[a]

[a] Sorbonne Universités, UPMC Univ Paris 06, CNRS, Collège de France, Laboratoire de Chimie de la Matière Condensée de Paris, 4 place Jussieu, 75005 Paris, France

[b] Sorbonne Universités, UPMC Univ Paris 06, CNRS, Collège de France, UMR 8260 "Chimie du Solide et Energie", Collège de France, 11 Place Marcelin Berthelot, 75231 Paris Cedex 05, France

[c] EDF R&D, 77818 Moret Sur Loing Cedex, France.

* Corresponding author at: Université Pierre et Marie Curie - LCMCP, 4 place Jussieu - 75252 Paris cedex 05, France. Tel.: +33 (0)1 44 27 56 79; Fax.: +33 (0)1 44 27 15 04.
E-mail address: damien.bregiroux@upmc.fr (D. Bregiroux)

Abstract

$Li_{1.3}Al_{0.3}Ti_{1.7}(PO_4)_3$ (LATP) materials are made of a three–dimensional framework of TiO_6 octahedra and PO_4 tetrahedra, which provides several positions for Li^+ ions. The resulting high ionic conductivity is promising to yield electrolytes for all-solid-state Li-ion batteries. In order to elaborate dense ceramics, conventional sintering methods often use high temperature (≥ 1000°C) with long dwelling times (several hours) to achieve high relative density (~ 90%). In this work, an innovative synthesis and processing approach is proposed. A fast and easy processing technique called microwave-assisted reactive sintering is used to both synthesize and sinter LATP ceramics with suitable properties in one single step. Pure and crystalline LATP ceramics can be achieved in only 10 min at 890 °C starting from amorphous, compacted LATP's precursors powders. Despite a relative density of 88%, the ionic conductivity measured at ambient temperature (3.15×10^{-4} $S.cm^{-1}$) is among the best reported so far. The study of the activation energy for Li^+ conduction confirms the high quality of the ceramic (purity and crystallinity) achieved by using this new approach, thus emphasizing its interest for making ion-conducting ceramics in a simple and fast way.

Keywords

NASICON, microwave – assisted reactive sintering, ceramics, ionic conductivity, Li-ion mechanism

1. Introduction

Solid state electrolytes are a cornerstone of solid oxide fuel cells, but also batteries and other various sensors (*e.g.* oxygen sensors, ion selective electrodes…) [1]. Among them, lithium ion conductors have attracted much attention, especially in the field of batteries [2]. Compared to organic electrolytes, inorganic lithium solid electrolytes exhibit higher electrochemical stability and lower flammability [3]. However, it is very challenging to reach Li^+ conductivity comparable to that achieved with organic electrolytes. Thus, in order to improve ionic conductivity, large efforts have been devoted to the development of new conductive materials and the optimization of their chemical composition. Several compounds have been identified as interesting inorganic solid state electrolytes for lithium ion conduction [4]. Among them, perovskite-type lithium lanthanum titanates (LLTO) [5,6], garnet-related oxides [7], lithium phosphorus oxynitride (LiPON) [8], sulphides ceramics and glass-ceramics [9,10], as well as NASICON-type aluminium-doped lithium titanium phosphate (LATP) [11-13], have been the subject of much research in recent years. The latter, with an optimized composition of $Li_{1.3}Al_{0.3}Ti_{1.7}(PO_4)_3$, is water stable and exhibits a conductivity of 7×10^{-4} $S.cm^{-1}$ at ambient temperature and a theoretical Ohmic resistance of 14 $\Omega.cm^2$ for a 100 μm–thick electrolyte [11]. The ionic conductivity of LATP ceramic electrolytes is strongly influenced by their microstructures (porosity, grain size, secondary phases…), which are controlled by the processing step [14]. For instance, because of the strong thermal expansion anisotropy of LATP, numerous microcracks are generated when the grain size is higher than a critical value, estimated to be around 1.6 μm [15]. Therefore, sintering processes should be chosen to keep grain sizes below this value. Fast and/or pressure-assisted sintering techniques, are then most favored. Spark plasma sintering was successfully used in the elaboration of fully dense LATP ceramics with limited grain growth [16,17]. Microwave (MW) sintering is another flash sintering technique that has many advantages compared to conventional and

SPS methods (low energy consumption, higher final relative density, possibility to sinter under a controlled atmosphere, all shapes available…) [18]. Moreover, the high heating rates that can be reached by MW sintering generally lead to finer and less defectives microstructures than those obtained by conventional sintering. As mentioned earlier, this is a key point for LATP ceramics.

The objective of the present work is to perform the synthesis and sintering of $Li_{1.3}Al_{0.3}Ti_{1.7}(PO_4)_3$ powder in one single step by using a monomode microwave furnace. Samples are characterized in terms of crystal structure, microstructure and Li ion conductivity. The advantages and drawbacks of the microwave technique for the elaboration of LATP solid electrolytes are then discussed in comparison with the other methods reported in the literature.

2. Experimental

Lithium carbonate (Li_2CO_3, Rectapur), anatase titanium dioxide (TiO_2, Sigma-Aldrich), aluminium oxide (Al_2O_3, Prolabo) and ammonium phosphate monobasic ($NH_4H_2PO_4$, Sigma-Aldrich) were weighted in stoichiometric ratio in order to synthesize $Li_{1.3}Al_{0.3}Ti_{1.7}(PO_4)_3$. Precursors were mixed in acetone by magnetic stirring for 2 hours. After evaporation of the solvent, the mixture was heated in a muffle furnace at 500 °C in air for 1 hour in an alumina crucible in order to evacuate the volatile compounds (CO_2, H_2O and NH_3). The mixture was dry-milled in air with a mixer ball-mill Retsch MM 400 in 25 mL zirconia jars (4 g per jar) with one 20 mm zirconia ball in each jar. To achieve homogeneous mixture, milling was repeated 7 times for 4 min at 20 Hz. The milled powder was then compacted in a 13-mm cylinder die under a 150 MPa compressive load. The as-synthesized pellet was then heated in air in a 2.45 GHz monomode micro-wave cavity (Sairem) at different powers and dwelling times. Samples were placed at the maximum of the electrical field, according to the protocol

previously described by Croquesel *et al.* [19,20]. The temperature was measured with a pyrometer located at around 20 cm of the surface of the pellet.

Powder X-ray diffraction (XRD) patterns were recorded using a Bruker D8-Advance diffractometer with Cu-K_α radiation source (λ_1=1.54056 Å, λ_2=1.54439 Å) equipped with a LynxEye detector. Temperature-dependent XRD data were collected using an Anton-Paar HTK 1200N furnace, both on heating and cooling between room temperature and 200 °C in 2θ range of 10 – 65 °. Rietveld refinements were performed using the FullProf program [21]. Specific surface area of the powder was measured by the BET method in N_2 with a Belsorp-Max apparatus. The bulk density of the sintered pellets was determined by geometrical measurements whilst considering a theoretical density of 2.95 g.cm^{-3}. FE-SEM microscopy with a S-3400N Hitachi apparatus was used to characterize the microstructures of the sintered pellets upon thermally etched surfaces. The ionic conductivity was measured on ~ 88% as-made ceramics (thickness = 1000 μm and diameter = 13 mm) using impedance spectroscopy. Prior to analysis, a gold thin layer was sputtered on the polished sides of the pellet to improve the electrical electrode/ceramic contacts. The measurements were performed at ambient temperature in air and at various temperatures (from 22 to 200 °C) to estimate the activation energy. The frequency range varied between 1 and 5.10^6 Hz with amplitude of 200 mV_{rms}. The equivalent electrical circuit used to extract the electrical parameters was Rohm-drop in series with Rct//CPEct in series with a Warburg element [22]. Zview software was used to analyze the spectra achieved at various temperatures. In this equivalent circuit, Rohm-drop represents the resistance of the Li-ion conducting ceramics whilst RcT//CPEct elements are related to the ceramic/gold interfaces and the gold electrodes.

3. Results and discussion

First, MW sintering tests were performed on a pellet made from the precursor mixture pre-calcined at 500 °C in air with no subsequent milling. During MW sintering, no shrinkage was observed and millimeter-sized pores were generated in the sample during heating. One can make the assumption that these pores originate from inhomogeneities present in the starting mixture. Phosphorus rich zones in the sample melt and decompose and therefore inhibit the densification of the pellet by generating porosity, as already observed on other phosphate ceramics [23]. In order to prevent this effect, the precursor mixture was milled prior to MW sintering (see Experimental section). Under these conditions, no large pores are formed and densification takes place. After milling, the starting mixture exhibits a specific surface area of 11 $m^2.g^{-1}$. SEM micrographs of the mixture pre-calcined at 500 °C, before and after milling are shown in Fig. 1 a and b, respectively. Agglomerates observed before milling are largely broken during the milling step. It can be noted that the mixture still contains some large agglomerates after milling, suggesting that this step still needs to be optimized, in particular by using more efficient milling techniques, *e.g.* planetary or attrition milling.

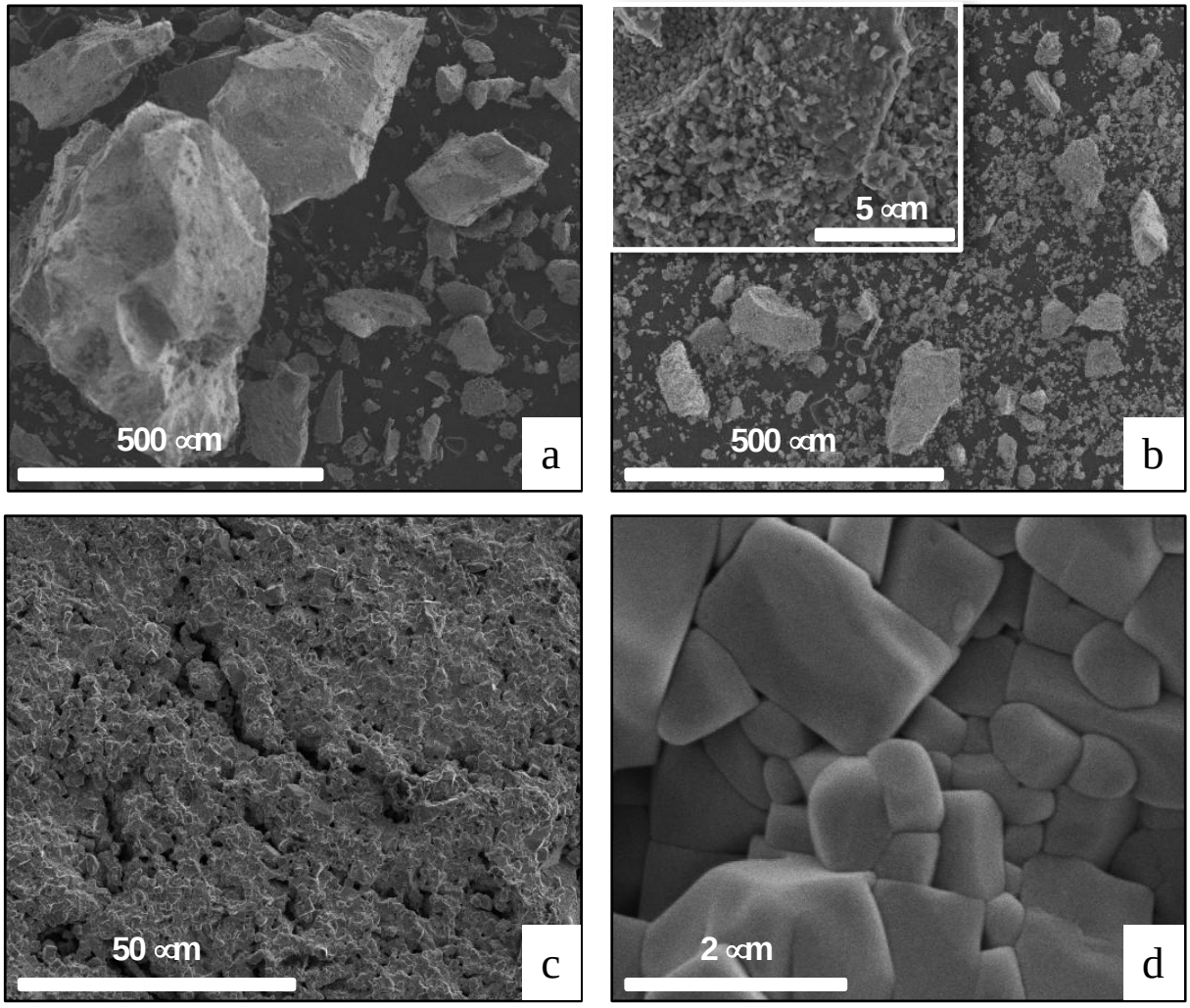

Fig. 1. SEM micrographs of the precursor mixture pre-calcined at 500°C for 1 h before (a) and after (b) milling, and of the materials after MW sintering of the milled precursors (shown in b) at 890 °C for 10 min (c and d)

The mixture pre-calcined at 500 °C in air was then pelletized and the pellet was finally sintered in the microwave furnace. XRD experiments were carried out on powders obtained from the precursor mixtures calcined at different temperatures (Fig. S1 in the SI). Between 500 °C and 800 °C, the materials mainly consist of a mixture of weakly crystallized LATP and TiP_2O_7. Above 900 °C, the high temperature structural form of $AlPO_4$ (trydimite $C222_1$) appears, as a consequence of the beginning of the decomposition of the LATP phase, according to the following reaction:

$$Li_{1+x}Al_xTi_{2-x}(PO_4)_3 \rightarrow \frac{3x}{4}Li_2O\uparrow + \frac{2-x}{2}LiTi_2(PO_4)_3 + xAlPO_4 + \frac{x}{8}P_4O_{10}\uparrow \quad (1)$$

Fig. 2 shows the Rietveld refinement of the hand-milled powder from a pellet sintered at 890 °C for 10 min. The only phase detected is LATP. Its cell parameters are consistent with those observed in the literature for the same composition [24,25]. Therefore, LATP is obtained as a pellet with very high purity. In the literature, $AlPO_4$ is very commonly observed, even as traces, in the XRD patterns [24,26,27]. Its action as a resistive layer is well-known and deleterious to ionic conductivity [28]. Here we show that MW-assisted reactive sintering enables producing pure LATP ceramics to be produced, probably because LATP cannot decompose in such a short processing time.

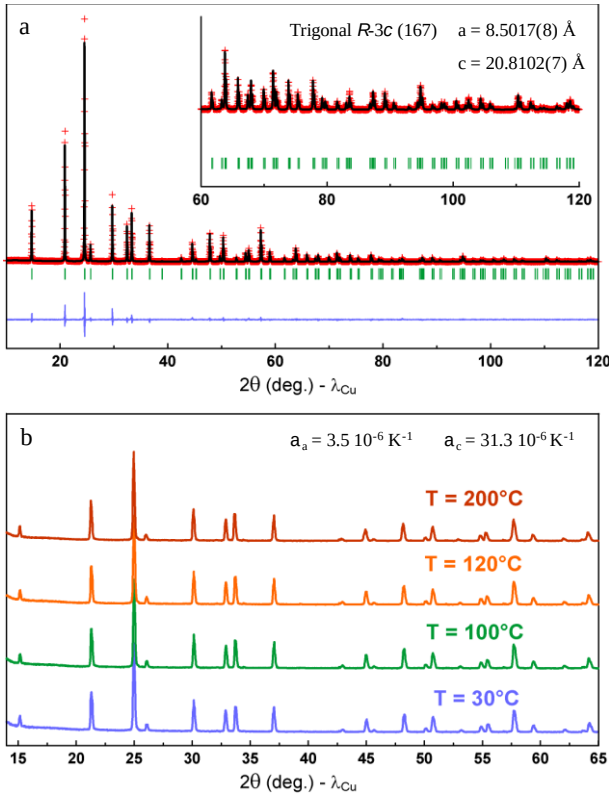

Fig. 2. (a) Rietveld refinement plot of LATP ceramic sintered at 890 °C for 10 min and then milled as a powder: observed Y_{obs} (red crosses), calculated Y_{calc} (black line), angular positions of Bragg reflections (vertical green bars) and difference curve Y_{obs} - Y_{calc} (blue line). (b) High

Temperature (HT)-XRD patterns of the same sample (as inset are given the linear thermal expansion coefficients derived from the cell parameters evolution).

Optimal sintering conditions are found to be at a temperature of 890 °C (*i.e.* 180 W absorbed for a 1 g pellet) and a dwell time of 10 min. The relative density is 88.2 % (81 % for a sintering temperature of 800 °C). No further densification is observed for longer dwell-time. The microstructures of the pellet after MW sintering at 890 °C for 10 min is shown in Figs. 1c and 1d. The morphological characteristics of the porosity observed in Fig. 1c. is typical of a sample made from an agglomerated powder. After sintering, agglomerates are well densified but inter-agglomerate porosity is still present in the sample (Fig. 1d). It can be expected that ceramics with higher final relative densities could be obtained with a starting powder with optimized morphological characteristics (*i.e.* smaller grain size with a narrower distribution). The microstructure consists of cubic-shaped grains with a mean grain size of 1.1 ± 0.4 μm. No secondary phase is observed by SEM at grain boundaries. It is worth noting that the mean grain size remains lower than the critical size of LATP (*i.e.* 1.6 μm, see Introduction).

Measurements of ionic conductivity and activation energy were carried out using impedance spectroscopy on a *ca.* 88 % dense LATP pellet sintered at 890 °C for 10 min at different temperatures ranging from room temperature to 200 °C under air. Fig. 3a gathers the Nyquist plot achieved at ambient temperature. At room temperature, the sample exhibits an ionic conductivity of $3.15\ 10^{-4}$ $S.cm^{-1}$. Such a conductivity value is high when compared to the literature (Fig. 3b), and considering the low value of the relative density of the ceramic. Such a high conductivity value is probably due to the absence of residual $AlPO_4$.

The conductivity follows an Arrhenius thermal activation process described by the following equation:

$$\sigma T = A \exp\left(\frac{-E_a}{RT}\right) \quad (2)$$

where σ is the ionic conductivity (S.cm^{-1}), T the temperature (K), A the pre-exponential term (T.S.cm^{-1}), E_a the activation energy (J.mol^{-1}) and R the gas constant (J.mol^{-1}.K^{-1}).

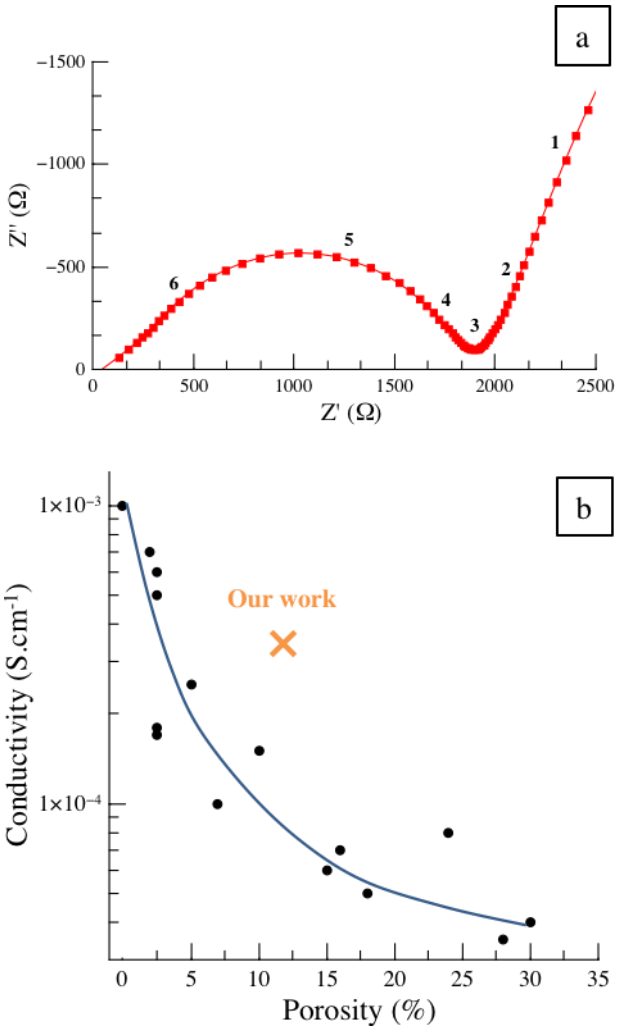

Fig. 3. (a) Nyquist plot of the LATP ceramic sintered at 890 °C for 10 min (the decades in frequency are mentioned), (b) Comparison of the Li ion conductivity of the same sample with the values reported in the literature and as a function of the porosity (data from Refs. [11-14,29-32].

A change of slope is observed at 135 °C in Fig 4a. Below this temperature, the activation energy is found to be 0.3 eV, which is in very good agreement with the values reported for the bulk conductivity in the literature in the same range of temperature [17,24,27]. At higher temperature, the activation energy increases to 0.53 eV. This modification can be related to a change in the conduction mechanism. High temperature XRD experiments were performed in order to track any structural modifications that can explain these changes. The XRD results are shown in Fig. 2b. No structural changes show up except the anisotropic cell thermal expansion. The latter is consistent with those reported in the literature [14].

Recent studies demonstrate that the Li-ion bulk conductivity of LATP is intrinsic in nature and is mainly based on the incorporation of the additional Li-ions as highly mobile charge carriers within the fast-diffusion pathways in the *R*-3*c* NASICON structure [33]. In this structure, lithium ions are located in two positions, namely M1 (*6b*) and M3 (*36f*), respectively (see [25] for more details on the LATP crystal structure). It has been unambiguously demonstrated recently that lithium ion conduction involves both sites according to a M1-M3-M3-M1 zig zag pathway (Fig. 4b) [33,34]. The corresponding activation energy, calculated from data obtained by the maximum-entropy method (MEM), is 0.30 eV (maximum entropy method), which is equal to the value obtained in this work below 135 °C. At higher temperature, the increase in the activation energy without structural modification indicates a change in the conduction mechanism. In the LATP NASICON structure, increasing temperature leads to a decrease of the M1 occupancy at the benefit of the M3 site. As the occupancies of M1 sites are reduced, a decoupled mechanism of diffusion of Li occurs, promoting the diffusion between Li located in M3 sites. The diffusion of Li from M3 to other M3 sites can occur even if the M3-M3 distance (3.60 Å) is higher than the M1-M3 distances (2.89 Å) (as shown on Fig. 4c), but with a higher energy barrier corresponding to the 0.53 eV measured in the present work. This diffusion path would then be possible only

with the aid of high temperatures (T higher than 135 °C), which can overcome the higher activation energy.

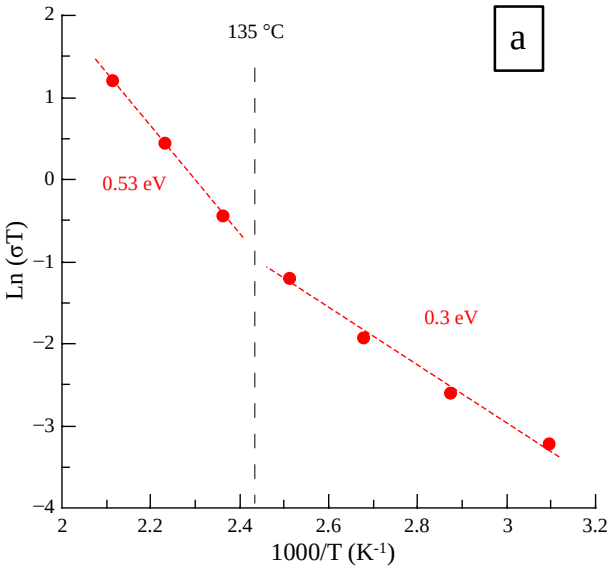
a
135 °C
0.53 eV
0.3 eV
Ln (σT)
1000/T (K-1)
2
1
0
−1
−2
−3
−4
2
2.2
2.4
2.6
2.8
3
3.2

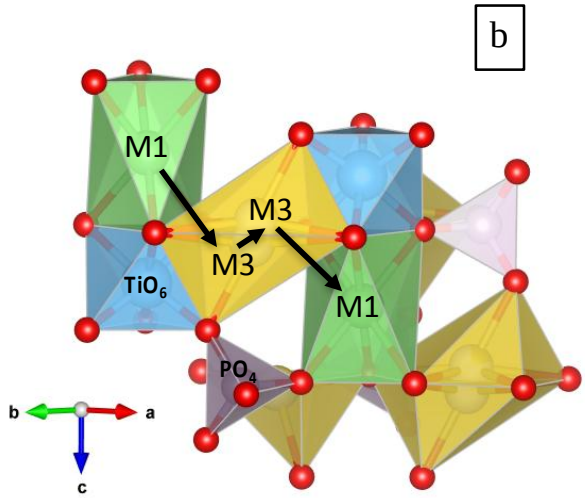
b
M1
M3
M3
M1
TiO6
PO4
b
a
c

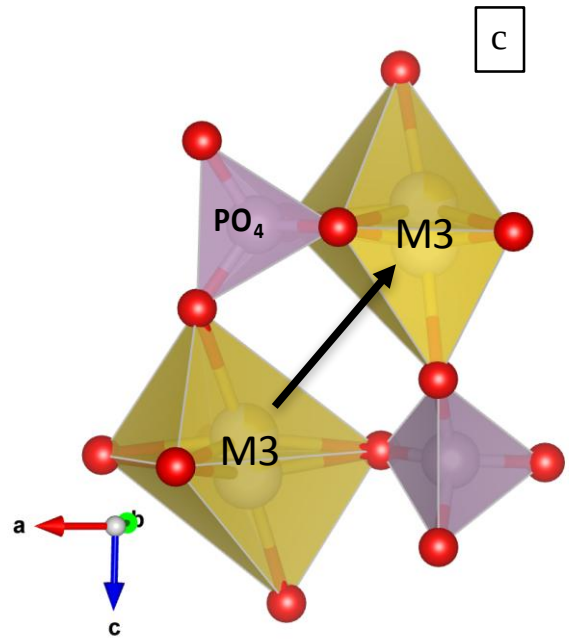
c
PO4
M3
M3
a
b
c

Fig. 4. (a) Arrhenius plot of the conductivity of the LATP ceramic sintered at 890 °C for 10 min, (b) Predominant Li conduction pathway at room temperature (according to Ref. [34]), (c) possible predominant Li conduction pathway at T > 135°C.

4. Conclusion

LATP are promising materials as electrolytes in all-solid-state Li-ion batteries because of their high Li-ion conductivity at low temperature. The synthesis of pure, dense LATP ceramics by an easy and fast processing technique called microwave-assisted reactive sintering has been investigated in order to synthesize and sinter LATP ceramics in a fast and single step. Moderately dense (88 %), crystalline and pure LATP ceramics, (without $AlPO_4$ impurities) consisting of cubic-shaped grains with a mean grain size of around 1 μm, have been obtained with a dwell-time of only 10 min at 850 °C. An ionic conductivity of 3.15×10^{-4} $S.cm^{-1}$ at room temperature has been measured by impedance spectroscopy. This value is among the best reported in the literature taking into account the relatively low density of 88%. Conductivity measurements performed at high temperature enabled the activation energy (E_a) to be measured. A change in E_a value has been highlighted corresponding to a modification of the Li-ion pathway. Further improvements in ionic conductivity are expected through the optimization of the sinterability of the precursors used for the fabrication of the green pellets.

Acknowledgment

This research did not receive any specific grant from funding agencies in the public, commercial, or not-for-profit sectors. The authors gratefully acknowledge Isabelle Genois for her help in SEM analysis and Alexandre Bahezre for his help for BET analysis.

Supporting Information

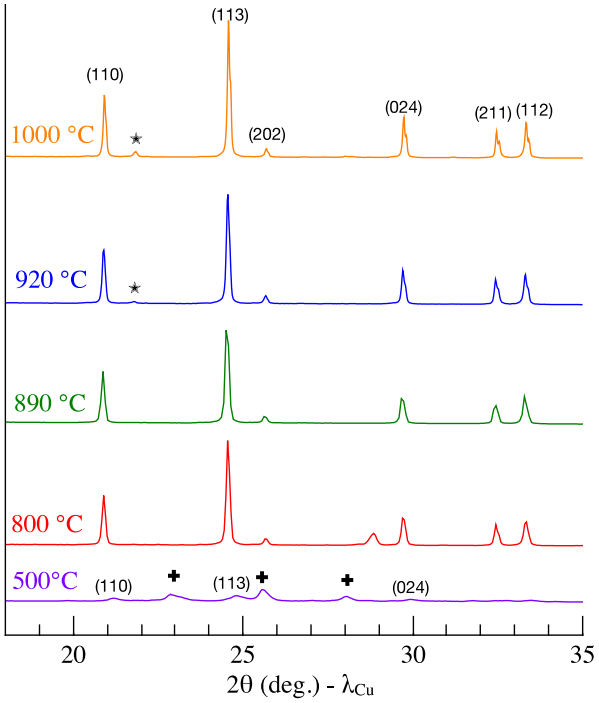

Fig. S1. XRD patterns of the precursor mixtures calcined at different temperatures with the microwave furnace (indexed peaks: $LiTi_2(PO_4)_2$ phase; stars: $AlPO_4$; crosses: TiP_2O_7)

References

[1] E.C. Subbarao, Solid Electrolytes and their Applications, Plenum Press, New York, 1980.

[2] Y. Ren, K. Chen, R. Chen, T. Liu, Y. Zhang, C.W. Nan, Oxide electrolytes for lithium batteries, J. Am. Ceram. Soc. 98 (2015) 3603-3623.

[3] Y. Wang, W.D. Richards, S. Ping Ong, L.J. Miara, J.C. Kim, Y. Mo, G. Ceder, Design principles for solid-state lithium superionic conductors, Nature Mater. 14 (2015) 1026–1031.

[4] C. Sun, J. Liu, Y. Gong, D.P. Wilkinson, J. Zhang, Recent advances in all-solid-state rechargeable lithium batteries, Nano Energy 33 (2017) 363-386.

[5] S. Stramare, V. Thangadurai, W. Weppner, Lithium lanthanum titanates: a review, Chem. Mater. 15 (2003) 3974-3990.

[6] K.P. Abhilash, P. Christopher Selvin, B. Nalini, K. Somasundaram, P. Sivaraj, A. Chandra Bose, Study of the temperature dependent transport properties in nanocrystalline lithium lanthanum titanate for lithium ion batteries, J. Phys. Chem. Solids 91 (2016) 114-121.

[7] Y. Li, J.T. Han, C.A. Wang, H. Xie, J.B. Goodenough, Optimizing Li^+ conductivity in a garnet framework, J. Mater. Chem. 22 (2012) 15357-15361.

[8] T. Pichonat, C. Lethien, N. Tiercelin, S. Godey, E. Pichonat, P. Roussel, M. Colmont, P.A. Rolland, Further studies on the lithium phosphorus oxynitride solid electrolyte, Mater. Chem. Phys. 123 (2010) 231-235.

[9] N. Kamaya, K. Homma, Y. Yamakawa, M. Hirayama, R. Kanno, M. Yonemura, T. Kamiyama, Y. Kato, S. Hama, K. Kawamoto, A. Mitsui, A lithium superionic conductor, Nat. Mater. 10 (2011) 682-686.

[10] M. Tatsumisago, A. Hayashi, Sulfide glass-ceramic electrolytes for all-solid-state lithium and sodium batteries, Int. J. Appl. Glass Sci. 5 (2014) 226-235.

[11] H. Aono, E. Sugimoto, Y. Sadaoka, N. Imanaka, G.Y. Adachi, Ionic conductivity of the lithium titanium phosphate ($Li_{1+x}M_xTi_{2-x}PO_4)_3$, M = Al, Sc, Y and La) systems J. Electrochem. Soc. 136 (1989) 590-591.

[12] H. Aono, E. Sugimoto, Y. Sadaoka, N. Imanaka, G.Y. Adachi, Ionic conductivity of solid electrolytes based on lithium titanium phosphate, J. Electrochem. Soc. 137 (1990) 1023-1027.

[13] G. Lancel, P. Stevens, G. Toussaint, M. Maréchal, N. Krins, D. Bregiroux, C. Laberty-Robert, Hybrid Li Ion Conducting Membrane as Protection for the Li Anode in an Aqueous Li−Air Battery: Coupling Sol−Gel Chemistry and Electrospinning, Langmuir, 33 (2017) 9288−9297.

under press (DOI: 10.1021/acs.langmuir.7b00675).

[14] T. Hupfer, E.C. Bucharsky, K.G. Schell, A. Senyshyn, M. Monchak, M.J. Hoffmann, H. Ehrenberg, Evolution of microstructure and its relation to ionic conductivity in $Li_{1+x}Al_xTi_{2-x}(PO_4)_3$ Solid State Ion. 288 (2016) 235-239.

[15] S.D. Jackman, R.A. Cutler, Effect of microcracking on ionic conductivity in LATP, J. Power Sources 218 (2012) 65-72.

[16] X. Xu, Z. Wen, X. Yang, L. Chen, Dense nanostructured solid electrolyte with high Li-ion conductivity by spark plasma sintering technique, Mater. Res. Bull. 43 (2008) 2334-2341.

[17] M. Pérez-Estébanez, J. Isasi-Marín, A. Rivera-Calzada, C. León, M. Nygren, Spark plasma versus conventional sintering in the electrical properties of Nasicon-type materials, J. Alloy. Compd. 651 (2015) 636-642.

[18] M. Oghbaei, O. Mirzaee, Microwave versus conventional sintering: A review of fundamentals, advantages and applications, J. Alloy. Compd. 494 (2010) 175-189.

[19] J. Croquesel, D. Bouvard, J.M. Chaix, C.P. Carry, S. Saunier, Development of an instrumented and automated single mode cavity for ceramic microwave sintering: Application to an alpha pure alumina powder, Mater. Des. 88 (2015) 98-105.

[20] J. Croquesel, D. Bouvard, J.M. Chaix, C.P. Carry, S. Saunier, S. Marinel, Direct microwave sintering of pure alumina in a single mode cavity: Grain size and phase transformation effects, Acta Mater. 116 (2016) 53-62.

[21] J. Rodriguez-Carvajal, FULLPROF.2k: Rietveld, Profile Matching and Integrated Intensity Refinement of X-ray and Neutron Data, V 1.9c, Laboratoire Léon Brillouin, CEA, Saclay, France, 2001.

[22] E. Barsoukov, J. Ross Macdonald, Impedance spectroscopy: Theory, experiment, and applications. 2nd Ed., Wiley, 2005.

[23] D. Bregiroux, S. Lucas, E. Champion, F. Audubert, D. Bernache-Assollant, Sintering and microstructure of rare earth phosphate ceramics *RE*PO_4 with *RE* = La, Ce or Y, J. Eur. Ceram. Soc. 26 (2006) 279-287.

[24] K. Arbi, W. Bucheli, R. Jiménez, J. Sanz, High lithium ion conducting solid electrolytes based on NASICON $Li_{1+x}Al_xM_{2-x}(PO_4)_3$ materials (M = Ti, Ge and $0 \leq x \leq 0.5$), J. Eur. Ceram. Soc. 35 (2015) 1477-1484.

[25] G.J. Redhammer, D. Rettenwander, S. Pristat, E. Dashjav, C.M.N. Kumar, D. Topa, F. Tietz, A single crystal X-ray and powder neutron diffraction study on NASICON-type $Li_{1+x}Al_xTi_{2-x}(PO_4)_3$ ($0 \leq x \leq 0.5$) crystals: Implications on ionic conductivity, Solid State Sci. 60 (2016) 99-107.

[26] K. Waetzig, A. Rost, U. Langklotz, B. Matthey, J. Schilm, An explanation of the microcrack formation in $Li_{1.3}Al_{0.3}Ti_{1.7}(PO_4)_3$ ceramics, J. Eur. Ceram. Soc. 36 (2016) 1995-2001.

[27] F. Ma, E. Zhao, S. Zhu, W. Yan, D. Sun, Z. Jin, C. Nan, Preparation and evaluation of high lithium ion conductivity $Li_{1.3}Al_{0.3}Ti_{1.7}(PO_4)_3$ solid electrolyte obtained using a new solution method, Solid State Ionics 295 (2016) 7-12.

[28] M. Kotobuki, M. Koishi, Preparation of $Li_{1.5}Al_{0.5}Ti_{1.5}(PO_4)_3$ solid electrolyte via a sol-gel route using various Al sources, Ceram. Int. 39 (2013) 4645-4649.

[29] C. Davis III, J.C. Nino, Microwave processing for improved ionic conductivity in Li_2O–Al_2O_3–TiO_2–P_2O_5 glass-ceramics, J. Am. Ceram. Soc. 98 (2015) 2422-2427.

[30] S. Duluard, A. Paillassa, L. Puech, P. Vinatier, V. Turq, P. Rozier, P. Lenormand, P.-L. Taberna, P. Simon, F. Ansart, Lithium conducting solid electrolyte $Li_{1.3}Al_{0.3}Ti_{1.7}(PO_4)_3$ obtained via solution chemistry, J. Eur. Ceram. Soc. 33 (2013) 1145-1153.

[31] Q. Ma, Q. Xu, C.-L. Tsai, F. Tietz, O. Guillon, A novel sol–gel method for large-scale production of nanopowders: Preparation of $Li_{1.5}Al_{0.5}Ti_{1.5}(PO_4)_3$ as an example, J. Am. Ceram. Soc. 99 (2016) 410-414.

[32] K.M. Kim, D.O. Shin, Y.-G. Lee, Effects of preparation conditions on the ionic conductivity of hydrothermally synthesized $Li_{1+x}Al_xTi_{2-x}(PO_4)_3$ solid electrolytes, Electrochim. Acta 176 (2015) 1364-1373.

[33] K. Arbi, M. Hoelzel, A. Kuhn, F. García-Alvarado, J. Sanz, Structural factors that enhance lithium mobility in fast-ion $Li_{1+x}Al_xTi_{2-x}(PO_4)_3$ ($0 \leq x \leq 0.4$) conductors investigated by neutron diffraction in the temperature range 100-500 K, Inorg. Chem. 52 (2013) 9290-9296.

[34] M. Monchak, T. Hupfer, A. Senyshyn, H. Boysen, D. Chernyshov, T. Hansen, K.G. Schell, E.C. Bucharsky, M.J. Hoffmann, H. Ehrenberg, Lithium diffusion pathway in $Li_{1.3}Al_{0.3}Ti_{1.3}(PO_4)_3$ (LATP) superionic conductor, Inorg. Chem. 55 (2016) 2941-2945.